ISBN 82-553-0332-4

Applied Mathematics
No 4 - December 7 1977

THREE-DIMENSIONAL LEE-WAVE PATTERN

by

B. Gjevik and T. Marthinsen
Oslo Oslo

PREPRINT SERIES - Matematisk institutt, Universitetet i Oslo

THREE-DIMENSIONAL LEE-WAVE PATTERN

B. Gjevik and T. Marthinsen
Institute of Mathematics
University of Oslo, Norway

Abstract

Satellite photographs are analysed in order to study the lee-wave pattern generated by isolated islands in the Norwegian Sea and the Barents Sea.

In situations where the wave motion is confined to the lower atmosphere (trapped waves) the waves are located within a wedge-shape wake behind the islands. Both the diverging wave type where the crests are orientated outward from the centre of the wake and the transverse wave type where the crests are nearly perpendicular to the wind direction are observed. The former wave type is, however, the most common wave type. In certain situations a long single-crested wave is observed at Jan Mayen. The wave appears on the photographs as a straight lane in the cloud layer. In one case it extends sidewise from the island to a distance of about 350 km. Wave kinematics is used to obtain the phase lines for steady wave pattern for different atmospheric models. The theory is found to explain some important features of the observed wave forms.

Introduction

A vast literature is available on atmospheric lee-waves. The most of it is concerned with waves generated by mountain ridges where the motion of an individual air particle is essentially confined to a vertical plane perpendicular to the ridge. The three-dimensional wave motion which occurs when the waves are generated by isolated mountain peaks, have received considerably less attention. A general mathematical treatment of this problem is very involved. The few works we know of, are Kochin (1938), Scorer and Wilkinson (1956), Wurtele (1957), Palm (1958), Crapper (1962), and Blumen & McGregor (1976). These works are mainly theoretical studies of the wave motion for rather special atmospheric situation, and the results are not compared with observations. The works by Kochin, Scorer and Crapper show that trapped waves are confined to a wedge-shape region behind the wave source and that the horizontal structure of the wave pattern is similar to the well-known ship-wave pattern. The waves are of two types: transverse waves with the wave crest nearly perpendicular to the wind direction, and diverging waves which radiate out from the wake. Scorer et.al. (1956) remark that the latter wave type is unlikely to be observed in the atmosphere.

We have studied satellite photographs of lee-waves generated by isolated islands in the Norwegian Sea and the Barents Sea and the observational results are presented in Section 2. Contrary to Scorer's statement the diverging wave type is found to be rather common.

Since the existing theoretical results refer to atmospheric models which are not applicable in our case, we have used wave kinematics to obtain the phase lines of the waves for more realistic atmospheric models. (Section 3). We have found that the theoretical results which

are based on linearized wave theory, explain many features of the observed wave pattern. There are, however, discrepancies between theory and observation and the theory is unable to explain the single-crested wave which can be observed at Jan Mayen in certain situations. This wave form has to our knowledge not previously been described in the literature.

2 Observational results

Studies of the satellite photographs show that three isolated islands in the Norwegian Sea and The Barents Sea often generate atmospheric lee-waves. These islands are Jan Mayen (71,0°N, 8.5°W), The Bear-Island (74.4°N, 19.0°E) and Hopen (76.6°N, 25.3°E). Waves are particularly frequent in the wake of Jan Mayen. This island is also known to generate vortex-streets and the vortex shedding at Jan Mayen has been studied by Wehner (1949), Mohr (1971) and Fjellheim (1973).

Before we proceed we will give a short description of the topography of the three islands.

In the eastern part of Jan Mayen a volcanic mountain, Beerenberg, rises to a height of 2277 m. The mountain is nearly conic with a diameter at the foot of about 15 km. Also the western part of the island is mountainous with the highest top at 769 m. The terrain between the mountains in the east and the west is low.

There is a low plateau at about 30-40 m in the north-western part of The Bear Island. The south-eastern part of the island is mountainous with three main peaks respectively at 536 m, 440 m and 360 m.

The island Hopen consists of a long narrow mountain ridge with mountain tops between 250 and 370 m.

In Fig. 1 the main topographical features of the three islands are shown.

On all three islands the Norwegian Meteorological Institute operates meteorological stations. From Hopen only surface observations are available, but from The Bear Island and Jan Mayen one also has regular upper air soundings.

We have examined VHRR-photographs in the visual and infrared band, taken by the satellites NOAA 4 and NOAA 5 in the period August 1976 to September 1977. Unfortunately, the photographs available to us are geometrically distorted, and data read from the photographs are corrected for the scale distortion. We have found lee-waves at Jan Mayen on 7 days, at The Bear Island on 2 days and at Hopen on 1 day. Vortex shedding at Jan Mayen occurred on 11 days.

Here we choose to present four cases with particular well developed lee-wave pattern. We believe that these cases demonstrate typical and general features of the wave motion and we will give an analysis of these cases.

Case I Jan Mayen, Sept. 1, 1976, about 11.17 GMT.

A photograph of the Jan Mayen region with a remarkable lee-wave pattern is shown in Figure 2a. The waves are visualized by a cloud layer, and the waves are clearly generated by the island's influence on the air flow. The snow-covered top of Beerenberg appears on the photograph as a white spot at the upstream front of the wave train.

Figure 3a shows a display of upper air data recorded by a radiosonde at nearly the same time as the photograph. These observations

show that a temperature inversion extends between a height of about 1400 m to about 2600 m and that the wind direction in the lower part of the atmosphere is nearly constant.

The surface observator reports cumulus and cumulonimbus clouds with cloud base at 300-600 m height. The radiosonding shows that the air above 1800 m is very dry, and that the cloud layer appearing on the photograph is formed by the horizontal spreading at the inversion.

A striking feature of the wave pattern is the lack of symmetry and this indicates that the terrain on the island has an important effect on the wave pattern.

The line formed by the converging wave crests at the centre of the wake corresponds closely to the wind direction above the cloud layer. We will therefore refer to this line which extends southward from the top of Beerenberg as the centre-axis of the wake.

A close inspection of the photograph reveals that an abrupt change in the wave-phase takes place along a straight line west of the centre-axis. This indicates that the wave pattern west of the centre-axis consists of two wave trains of different origin. The western wave train is most likely generated by the mountains on the western part of Jan Mayen while the wave train diverging out from the centre axis is generated by Beerenberg. The latter wave train is confined within a sector of about 17°. We measured the wave-length in the front of western wave train to about 9 km and found the wave crests to make an angle of about 30° with the centre axis. Assuming stationary wave crests, this leads to a phase velocity of about 18 m/s.

Within a sector of about 24° east of the centre axis and close to the island, there is a train of diverging waves. These waves are clearly generated by Beerenberg and they seem to be similar to the

waves generated on the western side of the mountain.

A straight dark lane in the cloud layer radiates from the eastern slope of Beerenberg to a distance of about 350 km from the island. The clearance in the cloud layer is most likely caused by downward motion of the air. The width of the lane is about 14 km and it makes an angle of about 52° with the wind direction. If the lane is stationary with respect to the ground, the propagation velocity relative to the air flow is about 27 m/s. Linear wave theory (see section 4) is unable to explain this high propagation velocity and also the fact that the lane appears to propagate with a nearly unchanged form. We suggest that this single crested wave may have a similar origin and structure as the solitary wave studied by Davis & Acrivos (1967). They found that a steady non-linear wave can propagate along an interfacial transition region between two homogeneous layers and that the propagation velocity for this wave increases with increasing amplitude of the wave.

Case II Jan Mayen, Dec. 29, 1976, 11.22 GMT.

Also on this photograph (Fig. 2b) a straight clear lane in the cloud layer radiates out from the eastern side of Jan Mayen where the snow-covered top of Beerenberg can be seen as a weak white spot. The wave length (width of the lane) is found to be about 14 km and it makes an angle of about 38° with the wind direction. The propagation velocity (with respect to the air) is found under the assumption that the lane remains stationary with respect to the island to be about 11 m/s. We note that although the wave-length is the same in Case I and Case II, the propagation velocity is considerably lower in the latter case.

The upper air data recorded at nearly the same time as the photograph is displayed in Fig. 3b. The wind direction varies little with height, and the wind is from the same direction as in Case I. As in Case I there is an low level temperature inversion, but in this case in only extend from 840 m to 1330 m above sea level.

The clouds over Jan Mayen are reported to be cumulus and cumulonimbus clouds, the cloud base is at 200-300 m. The air above 840 m is very dry and it is unlikely that the top of the clouds penetrates the inversion layer. Due to heating of the air over the sea, cloud bands and cloud cells associated with convection currents in the air are seen on the photograph.

A high cloud (white on the photograph) is formed over the south-western part of the island. It is an indication of strong vertical motion over the mountains in this part of the island. The wavy cloud band downwind from Beerenberg indicates that the wake is unstable and the atmospheric conditions are close to those which lead to vortex shedding. In other situations where a shallow stable layer intersects Beerenberg in a similar way as in this case, vortex shedding is frequent, (Fjellheim, 1973). The series of satellite photographs which we have examined, confirms this result. In none of these cases lee-waves are found to be excited.

Case III Jan Mayen, Oct. 8, 1976, 13.14 GMT.

In this case the wind is from east and there is an isothermal layer between 1720 m and 2600 m above sea level. (Fig. 3c). The cloud base (patches of stratus) is reported to be at 100-200 m with a layer of altocumulus clouds above. Above 1720 m the air is dry and we therefore assume that this level represents the top of the cloud layer.

The photograph (Fig. 2c) shows that these clouds are formed at the crests of the waves, and that a wake is formed by higher clouds (white on the photograph). The wave crests on the southern side of the wake extend further outward from the wake than the wave crests on the northern side of the wake. This may be an effect of the mountains on the southwestern part of Jan Mayen. A close inspection of the photograph also reveals a slight distortion of the wave crests. The waves on the northern side of the wake is confined within a sector of about 12°. If we disregard the distortion of the crests on the southern side of the wake, the wave pattern is remarkably symmetric on the two sides of the wake.

Case IV The Bear Island and Hopen, Sept. 19, 1976, 11.37 GMT.

The satellite photograph from the Spitzbergen region (Fig. 2d) shows two lee-wave patterns southeast of Spitzbergen. The northern of these patterns is generated by Hopen and the southern pattern by The Bear Island. Upper air data from The Bear Island recorded at about the same time as the photograph are presented in Fig. 3d. A strong temperature inversion extends between a height of about 700 m to a height of about 1500 m. Fog is observed at the ground and the air is saturated up to about 800 m. Above this level the air is dry. The waves are therefore most likely visualized by a cloud layer at about 800 m. The wind direction is from WNW and varies little with height. The wave pattern at The Bear Island consists of straight crested waves. The wave crests make an angle of about 65° with the wind direction. The wave crest on the northern side of the centre of the wake extends further out than on the southern side, and the former waves are confined to a sector of about 21°. This asymmetry in the wave pattern may be due to the shape and the location of the three

mountain tops on The Bear Island.

The average wave length measured along the centre of the wake is about 8.5 km.

The waves generated at Hopen is of the transverse wave type with wave crests almost perpendicular to the wind direction. The waves are confined within a sector of about 49° and the average wave length along the centre-axis of the wave train is about 9.5 km. There is no upper air data from Hopen. The temperature variation with height may be nearly the same as at The Bear Island. Since Hopen is located leeward of Spitzbergen, the wind speed at Hopen is, however, most likely lower than at The Bear Island.

The four cases examined here show typical although remarkable well developed lee-wave pattern. We note that the waves generated at Jan Mayen are of the diverging wave type and that waves of the transverse wave type are only observed at Hopen. The wave pattern generated at The Bear Island is difficult to classify to either of these groups. Other photographs show that the topography of this island seems to favour wave pattern of this special form.

3 The lee-wave pattern from a point source. Wave kinematics.

Whitham (1974) surveys the theory and gives some illustrative examples on how wave pattern can be obtained by kinematic arguments. We will use the same technique to obtain the form of the lee-wave pattern for atmospheric models. We describe the motion from a fixed Cartesian coordinate system. The axes x_1 and x_2 are horizontal and the former axis is along the direction of the wind. The wave field is assumed to be steady and the wave parametres are almost periodic functions of the coordinates x_1 and x_2. We denote the phase

function by $\psi(x_i)$ $(i = 1,2)$ and define a local wave number vector by

$$k_i = \frac{\partial \psi}{\partial x_i} \tag{3-1}$$

The vector k_i is therefore normal to curves of constant phase. The dispersion relation for linear waves is a functional relation between k_i and the physical parametres defining the state of the atmosphere. We write the functional relation in the form

$$D(k_i, U, N, H) = 0 \tag{3-2}$$

where U, N, H denote respectively the wind velocity, the Väisälä-Brunt frequency and the thickness of the layers in the atmosphere. (See Appendix). With the definition (3-1), equation (3-2) becomes a differential equation for ψ. This equation can be written in characteristic form

$$\frac{dx_i}{d\lambda} = \frac{\partial D}{\partial k_i} \; ; \qquad \frac{dk_i}{d\lambda} = - \frac{\partial D}{\partial x_i} \; ; \qquad \frac{d\psi}{d\lambda} = k_j \frac{\partial D}{\partial k_j} \tag{3-3}$$

This set of equations determines the characteristics $x_i = x_i(\lambda)$, the phase function ψ, and the wave number vector k_i in the horizontal plane. With horizontally uniform layers it follows that k_i is constant on the characteristics and for a point source the characteristics pass through this point. With the point source at origo, it follows from eq. (3-3) that

$$\frac{x_2}{x_1} = \left(\frac{\partial D}{\partial k_2} \Big/ \frac{\partial D}{\partial k_1} \right) \tag{3-4}$$

and

$$\psi = k_i x_i = 2n\pi \qquad (n = 0,1,2\cdots) \tag{3-5}$$

Eqs. (3-4) - (3-5) determine the phase lines.

The discontinuous model leads to a relatively simple expression for D (Appendix, eq. A1), and equations for the lines of constant phase can be obtained easily from eq. (3-4) and (3-5). We find

$$\frac{x_1}{H} = p\,\frac{F^2\cos^3\varphi(1-F^2\cos^2\varphi+2\tg^2\varphi)}{(1-F^2\cos^2\varphi)^2}$$

$$\frac{x_2}{x_1} = -\,\frac{\tg\varphi(1+F^2\cos^2\varphi)}{1-F^2\cos^2\varphi+2\tg^2\varphi} \qquad (3\text{-}6)$$

where $p = 2\left(\frac{U_1}{U_0}\right)^2 n\pi$ and $-\frac{\pi}{2} < \varphi < \frac{\pi}{2}$. F is the Froude number. In the limit $H \to \infty$, $F \to 0$ and eq. (3-6) reduces to the well-known equation for the phase lines for ship-waves in deep water. For F and H finite the phase lines obtained from eq. (3-6) are similar to the phase lines for ship-waves in shallow water. For $F < 1$ both transverse and diverging waves are possible. For $F > 1$ there will only be diverging waves. The waves are confined within a wedge-shape region behind the wave source and the wedge-angle vary in a similar way as for ship-waves in shallow water. Subsequently we denote the semi wedge-angle by θ. For $F \neq 0, (H \to \infty)$ $\theta = 19.47^\circ$, for $F = 1$, $\theta = 90^\circ$ and for $F \to \infty$, $\theta \to 0$.

Although the discontinuous model reveals characteristic features of the wave pattern, the model is too simple for a direct comparison with the observational result in Section 2. We have therefore investigated the properties of different four layer models. The dispersion relation for a four layer model is given in eq. A2 in the Appendix. This equation together with eqs. (3-4) and (3-5) determine the phase lines which are evaluated by numerical methods.

In Figs. 4a and 4b the computed values of the semi wedge-angle, θ, as a function of the Scorer-parameter, γ, for the most stable layer are depicted. For these computations we have used layer thickness corresponding respectively to Case III and Case IV (See Table I) . In Figs. 4a and 4b these models are marked by a dot.

The curves label A (full line, 1.mode, dotted line, 2.mode) correspond to a model with $\gamma_0 = \gamma_2 = \gamma_3 = 0$, i.e. a three layer model where a stable layer is inbedded between two neutrally stable layers. For a certain value, $\gamma_1 = \gamma_{1m}$, say, the angle θ for the 1.mode approaches 90°. The diverging wave type is the only possible wave form for $\gamma_1 < \gamma_{1m}$. For $\gamma_1 > \gamma_{1m}$ both diverging and transverse waves are possible.

If the stability of the two upper layers are increased, the value of θ decreases. This effect is illustrated by the curves labeled B and C. The stable stratification of the upper layers allows long waves to propagate vertically and trapped waves are possible only for γ_1 above a certain value and for wave-length shorter than a certain cut-off. For simplicity reasons we denote $\gamma_1 \cdot 10^3 m$ by γ_1. In case B Fig. 4a the diverging waves are the only possible wave form when $0.3 < \bar{\gamma}_1 < 0.6$. For $0.6 < \bar{\gamma}_1 < 1,1$ both diverging and transverse waves are possible. The transverse waves disappear in a sector which includes the centre of the wake. For $\bar{\gamma}_1 > 1.1$ there is no cut and both wave types are possible. Case C, Fig. (4a), is similar. For $0.5 < \bar{\gamma}_1 < 1.0$, diverging waves, for $1.0 < \bar{\gamma}_1 < 1.2$, diverging and transverse waves, the latter waves disappear near the centre of the wake, and for $\bar{\gamma}_1 > 1.25$, diverging and transverse waves.

In the cases B and C, Fig. (4b), the diverging and transverse waves are possible for $\bar{\gamma}_1 > 1.25$ and $\bar{\gamma}_1 > 1.45$ respectively. For $0.4 < \bar{\gamma}_1 < 1.2$, and $0.7 < \bar{\gamma}_1 < 1.4$, respectively, in case B and C, both types is possible and the transverse waves are cut.

For the range of parametres treated in Fig. (4a) and (4b) the diverging wave type is the only possible wave form for the 2. mode.

The graphs corresponding to this mode are drawn by dotted lines.

For other four-layer models we have found quantitatively similar results as summarized in Figs. 4a and 4b.

4 Comparison between theory and observations

It should be stressed that the kinematic arguments give possible steady wave pattern due to a point source.

In order to determine uniquely which wave type is excited, the amplitudes of the waves have to be evaluated. This is a formidable problem which also requires a realistic representation of the topography of the wave source. The photographs of the wave pattern in Case I-IV indicate that at least in some of these situations the waves appear to be generated by a point source. We have therefore evaluated possible steady wave pattern for atmospheric models corresponding to Case I-IV by the methods of section 3.

Since the wave motion is confined to the lower part of the atmosphere, we have disregarded the strong stability of the stratosphere. If this effect had been included in the models, the main effect would be a weak damping of the wave field in the horizontal direction (slightly leaky waves).

The value of the parametres for the four models are given in Table I.

Table I

Case	$\frac{U}{U_0}$	H_0 km	H_1 km	H_2 km	$\gamma_0 \cdot 10^3$ m^{-1}	$\gamma_1 \cdot 10^3$ m^{-1}	$\gamma_2 \cdot 10^3$ m^{-1}	$\gamma_3 \cdot 10^3$ m^{-1}
I	1.1	0.9	1.7	2.0	0.2	0.5	0	0.2
II	0.8	0.8	0.5	-	0.3	1.5	0.6	-
III	0.8	1.7	0.9	6.7	0	0.9	0.4	0.5
IV	1.0	0.7	0.8	1.7	0	1.5	0.3	0.55

The phase-line pattern corresponding to these four models are displayed respectively in Fig. 5 a-d.

Case I The computed wave pattern consists mainly of diverging waves (Fig. 5a) and the semi wedge-angle is 17.8°. Also the photograph (Fig. 2a) shows a well developed train of diverging waves especially on the western side of the centre-axis of the wake. The part of the wave-train generated by Beerenberg seems to be confined within a wedge (See under Case I, section 2) and the wedge-angle and the length of the waves are in close agreement with the waves in Fig. 5a. The part of the wave-train generated by the mountains in the western part of the island are also confined within a wedge of similar width.

Fig. 5a shows that all the linear wave components of this model propagate relatively slow and the model is therefore unable to explain the existence of the single-crested wave east of Jan Mayen. (Fig. 2a). This leads us to suggest that the wave may be an internal solitary wave (See under Case I, section 2).

Case II The steady wave pattern (Fig. 5b) consists mainly of diverging waves. The semi wedge-angle is 15.3° and the wave-length is shorter than 5 km. The diverging wave type is not observed in this case nor in other similar situations (See under Case II, section 2). These results indicate that wave components shorter than 5 km, say, is unlikely to be excited when a relatively thin stable layer intersects Beerenberg well below the summit.

As in Case I the model is unable to explain the existence of the single-crested wave which can be seen east of Jan Mayen (Fig.2b).

Case III In this case the steady pattern (Fig. 5c) consists only of diverging waves and the semi wedge-angle is 10.7°. This wave type

is also observed (Fig. 2c). The computed semi wedge-angle agrees well with the observed angle for the wave train north of the wake. The wave train south of the wake extends over a wider sector but this is most likely an effect of the mountains on the western part of the island (See under Case III, section 2). We note that the observed wave length at the outer edge of the wedge compares well with the waves in Fig. 5c. The observed wave length near the centre of the wake is, however, somewhat larger than for the waves in Fig. 5c.

Case IV In this case the computation leads to a wave pattern which consists both of diverging waves and well developed transverse waves (Fig. 5d). The semi wedge-angle is 21.7° and the wave length of the transverse waves is about 10 km. The wave length of the diverging waves is shorter. The transverse wave train compares relatively well with the observed wave train at Hopen. The straight-crested wave train generated at The Bear Island differs, however, from either of the wave trains in Fig. 5d. We note that the second mode for this model leads to straight crested waves, but other features of the wave train for this mode are in disagreement with the observation. The waves observed at The Bear Island may therefore be strongly effected by the topography of the island or eventually by a wind defect in its wake.

Acknowledgement

The satellite photographs used in this study are provided by Tromsø Satellitt- Telemetristasjon, NTNF, Tromsø, Norway, and the meteorological data are provided by Norges Meteorologiske Institutt, Blindern, Norway.

We acknowledge the kindness and the expediency our many requests to these institutions have been met with.

APPENDIX

We assume that the three-dimensional wave motion is steady, adiabatic and frictionless. The governing equation for this motion is given by the authors referred to in the introduction, and it is no need for recapitulating it here.

Since the wind velocity, U, changes relatively slowly with height in all the cases we examine, we assume that the Scorer-parametre $\gamma = N/U$ (N is the Väisäla-Brunt frequency) is the only parametre needed for determining the motion. In the usual way we define layers with constant γ and the requirement of no vertical motion at the ground, $x_3 = 0$, and for $x_3 \to \infty$ defines a well-known eigenvalue-problem which in turn leads to the dispersion relations given below.

Subsequently we denote the length of the horizontal wave number vector by k and we introduce an angle φ defined by $\cos\varphi = -k_1/k$.

i) Discontinuous model: A neutrally stable atmosphere above and below an infinitely thin inversion.

We set $N = 0$, $U = U_0$ for $0 < x_3 < H_0$ and $N = 0$, $U = U_1$ for $x_3 > H_0$ and denote the relative density difference at the inversion layer by ε, ($\varepsilon \ll 1$). The dispersion relation for this model is

$$D = 1 + \left(\frac{U_1}{U_0}\right)^2 \operatorname{Tan} kH_0 - \frac{1}{F^2\cos^2\varphi}\,\frac{\operatorname{Tan} kH_0}{kH_0} = 0 \qquad \text{(A 1)}$$

where $F = U_0/\sqrt{\varepsilon g H_0}$ is the Froude number. With $\operatorname{Tan} kH \simeq kH$ an approximation to (A 1) valid also for kH considerably larger than unity is obtained. This approximation is used for evaluating the phase lines eq. (3-6).

ii) 4 layer model: The thickness of the three lower layers are denoted H_i ($i = 0,1,2$; numbered from the ground). The fourth and upper layer extends to infinity. The value of the Scorer-parametre in the four layers is respectively γ_i ($i = 0,1,2,3$). We allow for discontinuity in the wind velocity at $x_3 = H_0$ and set $U = U_0$ for $x_3 = H_0-$ and $U = U_1$ for $x_3 = H_0+$. With this notation the dispersion relation reads :

$$D = q_2\left(q_0 \frac{\operatorname{tg} q_1H_1}{q_1} + \left(\frac{U_1}{U_0}\right)^2 \operatorname{Tan} q_0H_0\right)\left(q_3 + q_2 \operatorname{Tan} q_2H_2\right)$$
$$+ \left(q_0 - q_1\left(\frac{U_1}{U_0}\right)^2 \operatorname{Tan} q_0H_0 \operatorname{tg} q_1H_1\right)\left(q_2 + q_3 \operatorname{Tan} q_2H_2\right) \qquad \text{(A 2)}$$

where

$$q_1 = \left[\left(\frac{\gamma_1}{\cos\varphi}\right)^2 - k^2\right]^{\frac{1}{2}}$$

and

$$q_i = \left[k^2 - \left(\frac{\gamma_i}{\cos\varphi}\right)^2\right]^{\frac{1}{2}} \quad \text{for} \quad i = 0,2,3.$$

For the trapped wave modes we consider, all the q_i are real.

REFERENCES

1 Blumen, W. and Cary D. McGregor (1976) Tellus 28, 287.

2 Crapper, G.D. (1962) Phil.Trans Roy. Soc. London Series A 254, 601.

3 Fjellheim, K.W. (1973) Technical Report No. 16. Norwegian Meteorological Institute. (In Norwegian).

4 Kochin (1938) Trudy Glav. Geofiz. Observ. 8, 3 = Sobranie Sochineini TI p.478 Akad.Nauk. SSSR Moscow-Leningrad 1949 (In Russian).

5 Mohr, T. (1971) Met. Rdsch 24, 30.

6 Palm, E. (1958) Geof. Publ. (Oslo) Vol. XX, No. 3.

7 Scorer, R.S. and Mary Wilkinson (1956) Quart.J.R.Met.Soc. 82, 419.

8 Wehner, H. (1949) Dissertation Universität Leipzig Akademie-Verlag, Berlin.

9 Whitham, G.B. (1974) Linear and Nonlinear Waves, John Wiley & Sons, New York.

10 Wurtele, M.G. (1957) Beitr. Phys. Atmos. 29, 242.

FIGURE CAPTIONS

Figure 1 Maps of Jan Mayen, The Bear Island and Hopen showing the main topographical features of the islands.

Figure 2 Section of a VHRR-photograph taken by NOAA 5 . The scale indicates the flight direction of the satellite. The scale perpendicular to the flight direction is subpressed by a factor: 0.72

2a; Jan Mayen Sept. 1. 1976, 11.17 GMT (visual band) On the left side Scoresby Sound on East-Greenland.

2b; Jan Mayen Dec. 29. 1976, 11.22 GMT (infrared band).

2c; Jan Mayen Oct. 8. 1976, 13.14 GMT (infrared band).

2d; Spitzbergen Sept. 19. 1976, 11.37 GMT (visual band).

Figure 3 Upper air data on temperature (solid lines), dew-point temperature (dotted lines), wind (direction and force, in kns.) and stability (N). In the temperature diagram (left) wet adiabats are drawn by —°— and dry adiabats by — — — .

3a; Jan Mayen Sept. 1. 1976, 11.15 GMT - 12.20 GMT.

3b; Jan Mayen Dec. 29. 1976, 11.15 GMT - 11.53 GMT.

3c; Jan Mayen Oct. 8. 1976, 11.15 GMT - 12.27 GMT.

3d; The Bear Island Sept. 19. 1976, 11.15 GMT - 12.34 GMT.

Figure 4a The semi wedge-angle, θ, as function of γ_1 for models with $U/U_0 = 0.8$, $H_0 = 1700$ m, $H_1 = 900$ m and $H_2 = 6700$ m. A: $\gamma_0 = \gamma_2 = \gamma_3 = 0$. B: $\gamma_0 = 0$, $\gamma_2 = 0.2 \cdot 10^{-3} m^{-1}$, $\gamma_3 = 0.3 \cdot 10^{-3} m^{-1}$. C: $\gamma_0 = 0$, $\gamma_2 = 0.4 \cdot 10^{-3} m^{-1}$ and $\gamma_3 = 0.5 \cdot 10^{-3} m^{-1}$. Solid lines and dotted lines correspond respectively to the 1. mode and the 2. mode. Case III is marked with a dot.

Figure 4b The semi wedge-angle, θ, as function of γ_1 for models with $U/U_0 = 1.0$ for models with $H_0 = 700$ m, $H_1 = 800$ m, $H_2 = 1700$. A: $\gamma_0 = \gamma_2 = \gamma_3 = 0$. B: $\gamma_0 = 0$, $\gamma_2 = 0.2 \cdot 10^{-3} m^{-1}$, $\gamma_3 = 0.3 \cdot 10^{-3} m^{-1}$. C: $\gamma_0 = 0$, $\gamma_2 = 0.3 \cdot 10^{-3} m^{-1}$ and $\gamma_3 = 0.55 \cdot 10^{-3} m^{-1}$. Solid lines correspond respectively to the 1.mode and the 2. mode. Case IV is marked with a dot.

Figure 5 Phase-lines for Case I - IV displayed respectively in a - b. The phase difference between corresponding points on neighbouring lines are 2π.

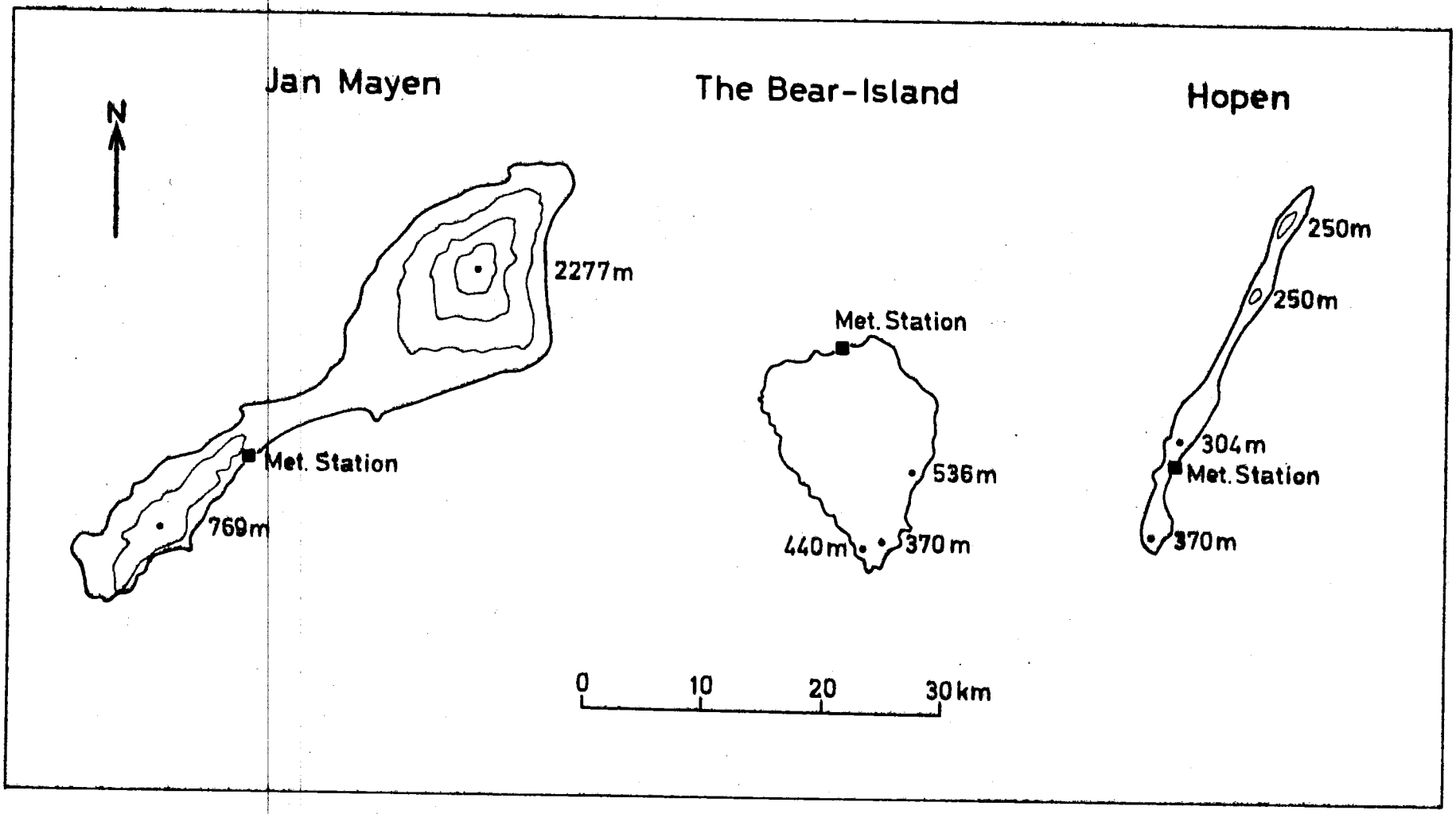
Jan Mayen
The Bear-Island
Hopen
N
2277m
Met. Station
769m
Met. Station
536m
440m
370m
250m
250m
304m
Met. Station
370m
0
10
20
30 km

Fig. 1

Figure 2a

Figure 2b

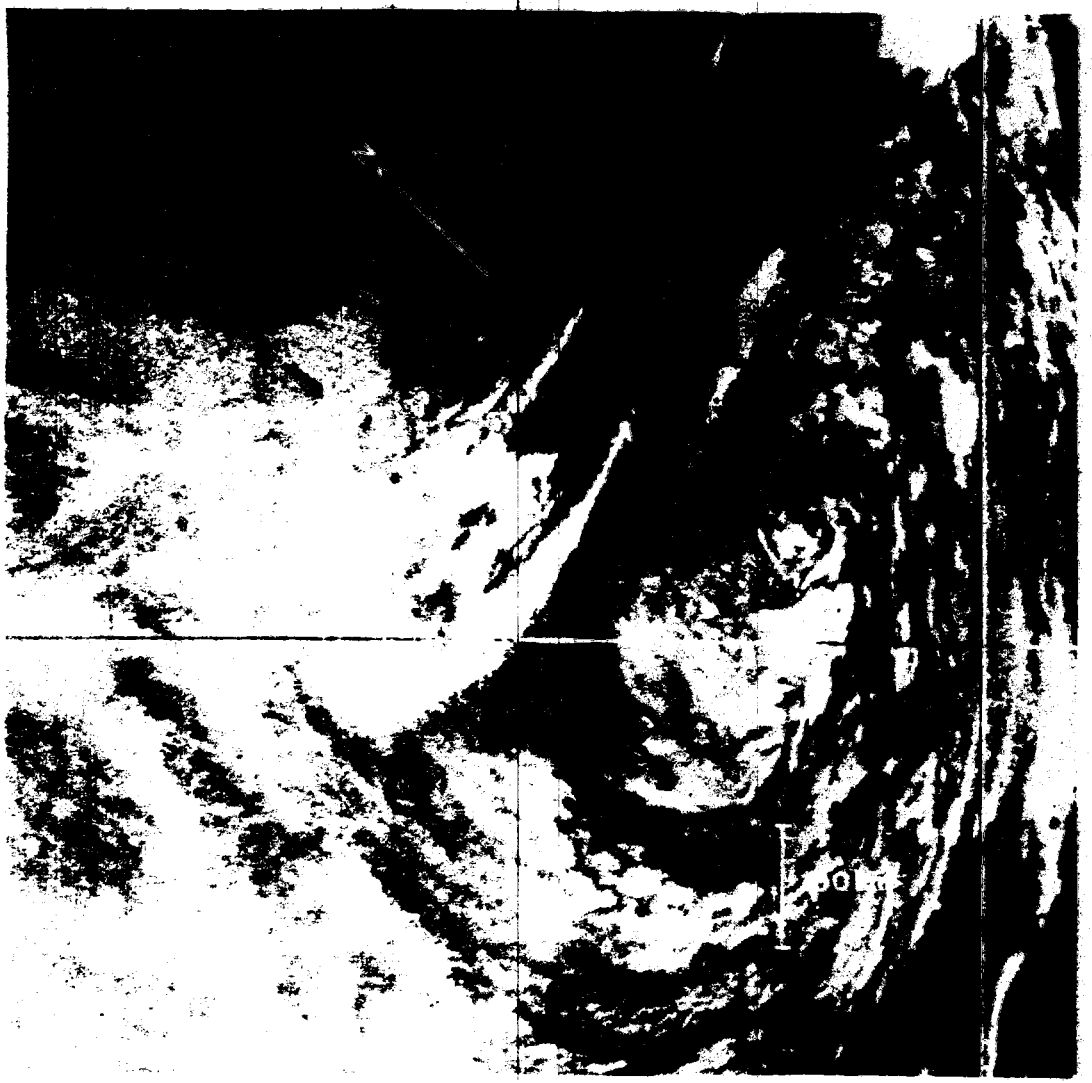

Figure 2c

Figure 2d

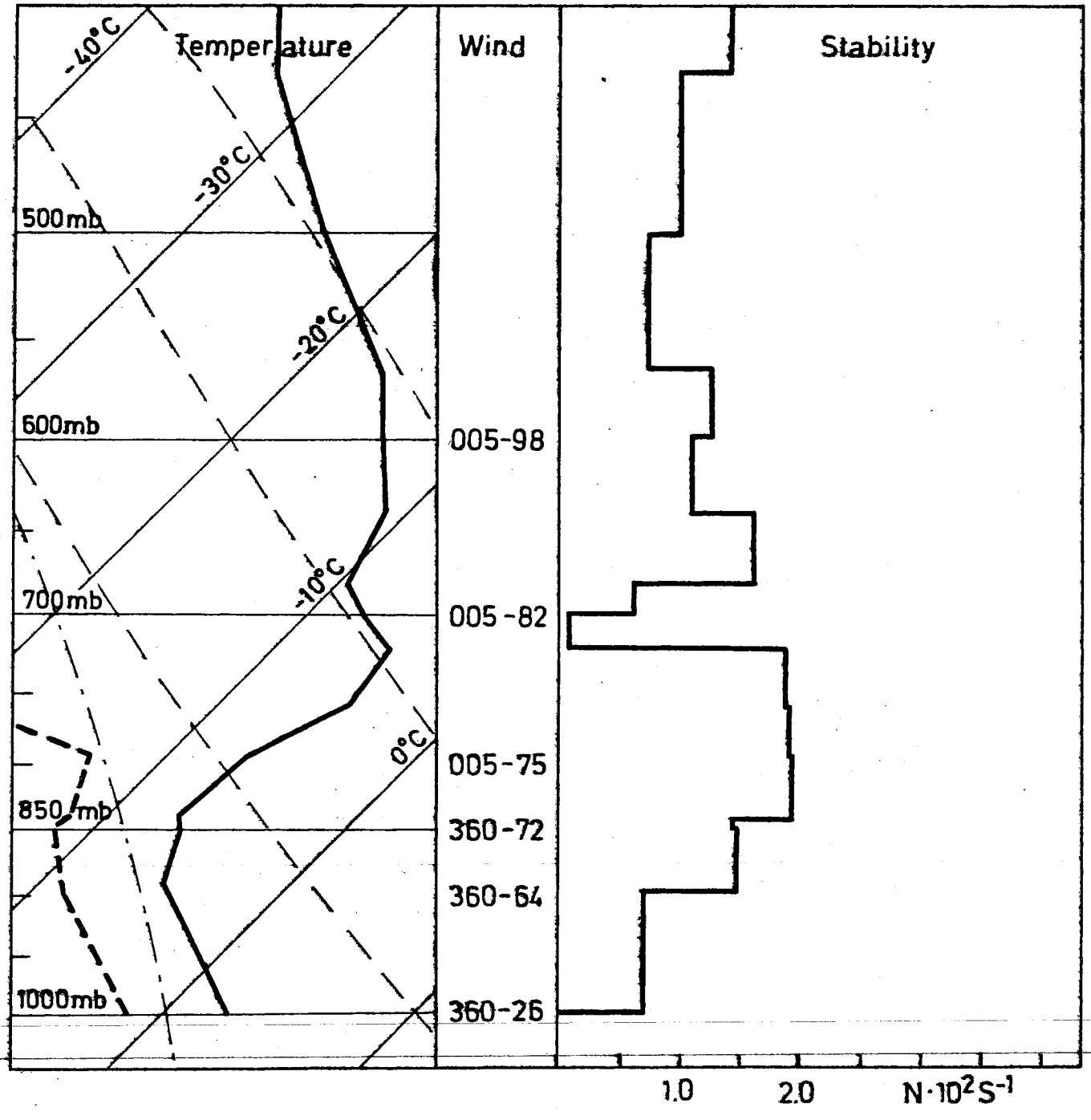
Temperature
Wind
Stability
-40°C
-30°C
-20°C
-10°C
0°C
500mb
600mb
700mb
850mb
1000mb
005-98
005-82
005-75
360-72
360-64
360-26
1.0
2.0
N·10²S⁻¹

Fig. 3a

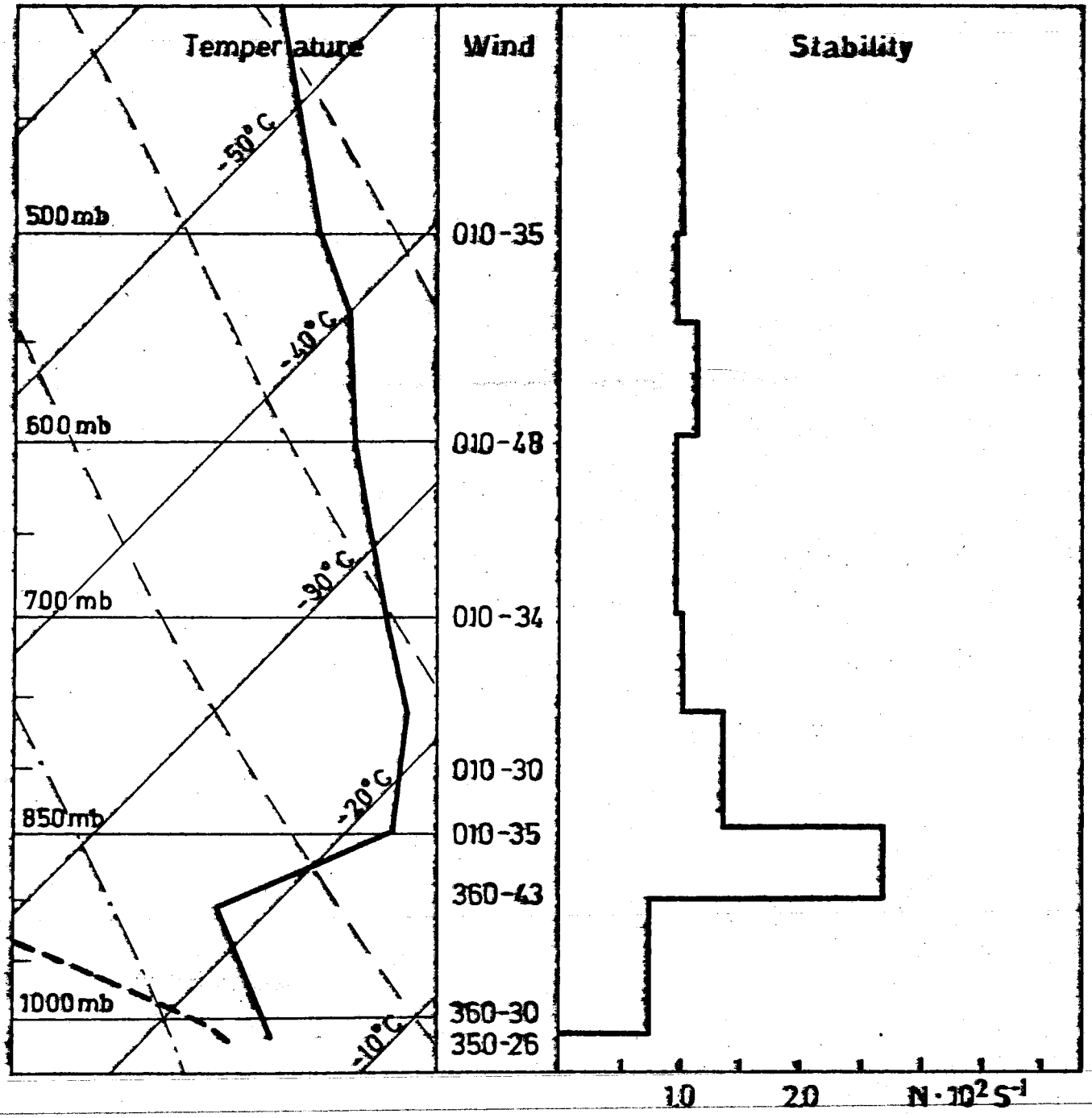
Temperature
Wind
Stability
-50°C
-40°C
-30°C
-20°C
-10°C
500 mb
600 mb
700 mb
850 mb
1000 mb
010-35
010-48
010-34
010-30
010-35
360-43
360-30
350-26
1.0
2.0
N·10² S⁻¹

Fig. 3b

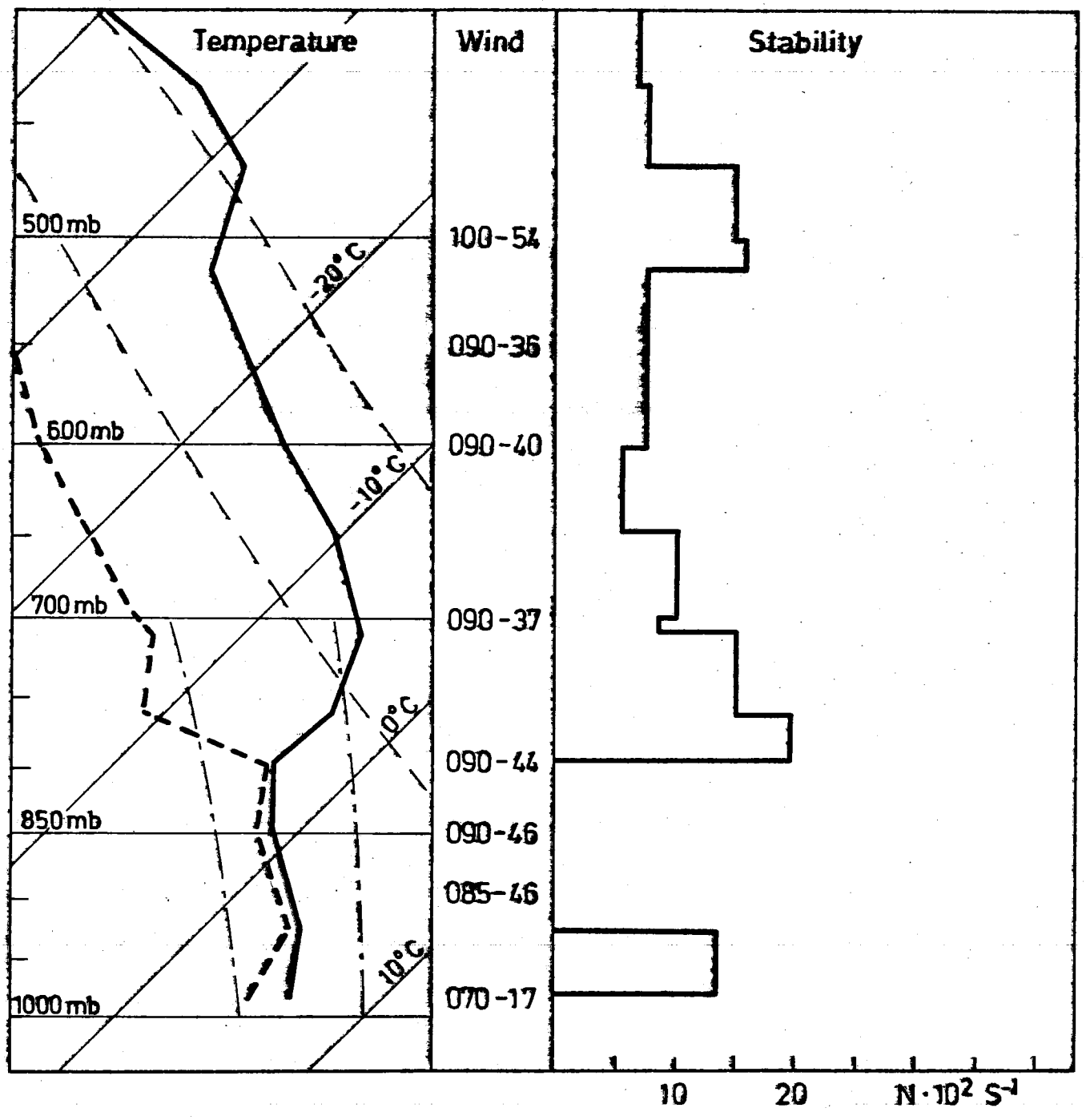
Temperature
Wind
Stability
500 mb
600 mb
700 mb
850 mb
1000 mb
-20°C
-10°C
0°C
10°C
100-54
090-36
090-40
090-37
090-44
090-46
085-46
070-17
10
20
N·10² S⁻¹

Fig. 3c

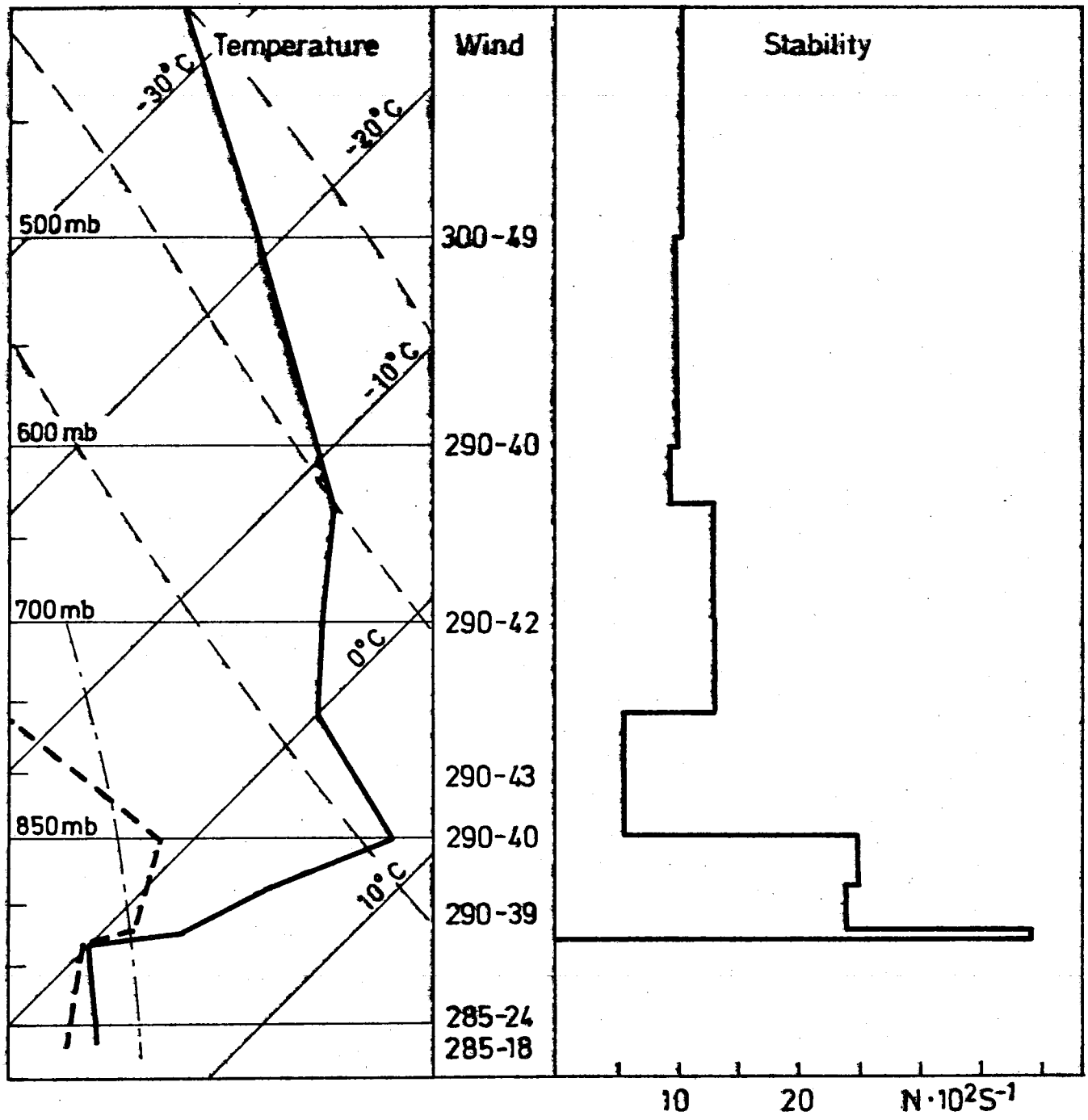
Temperature
Wind
Stability
-30°C
-20°C
-10°C
0°C
10°C
500mb
600mb
700mb
850mb
300-49
290-40
290-42
290-43
290-40
290-39
285-24
285-18
10
20
N·10²S⁻¹

Fig. 3d

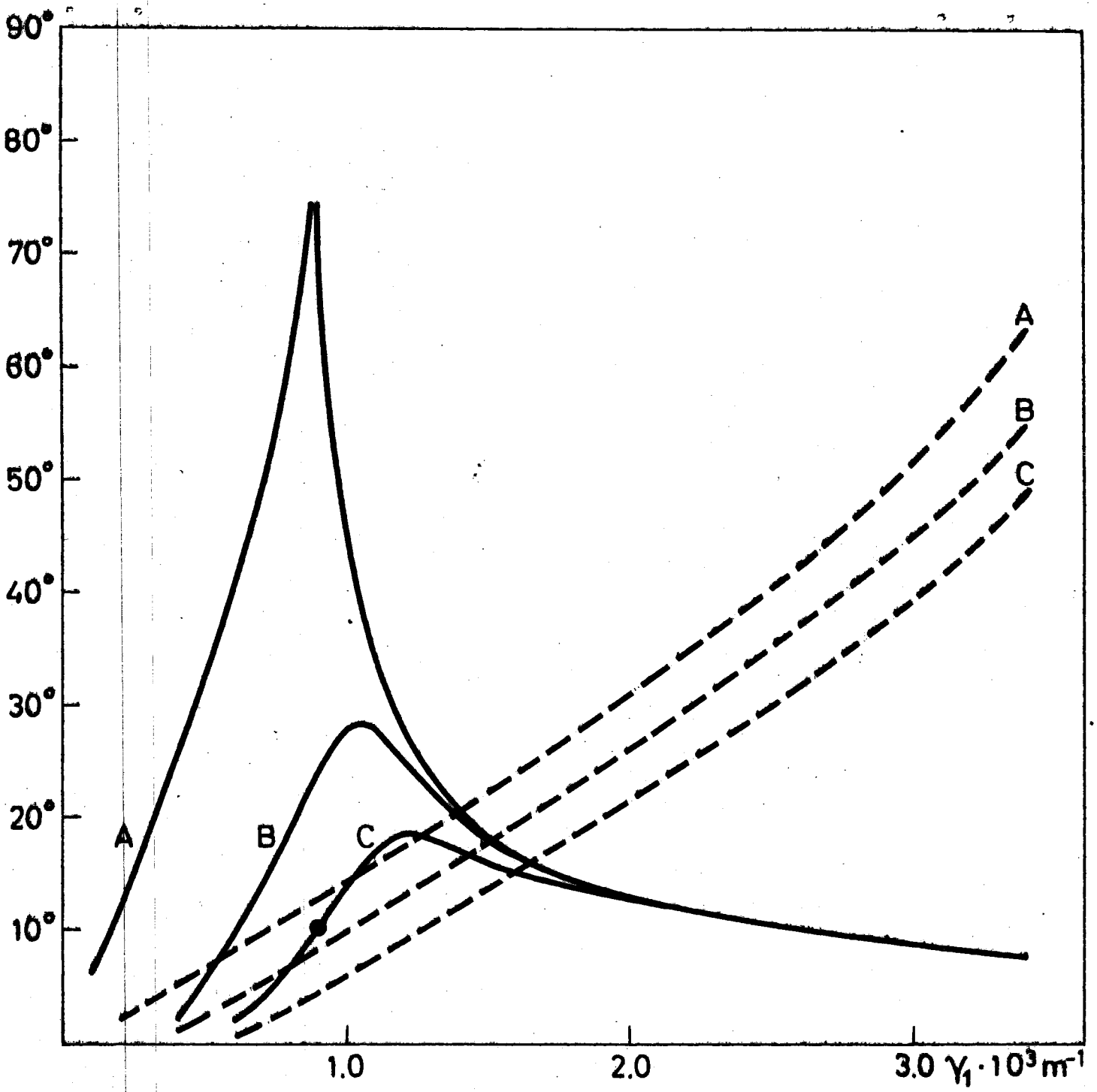

Fig. 4a

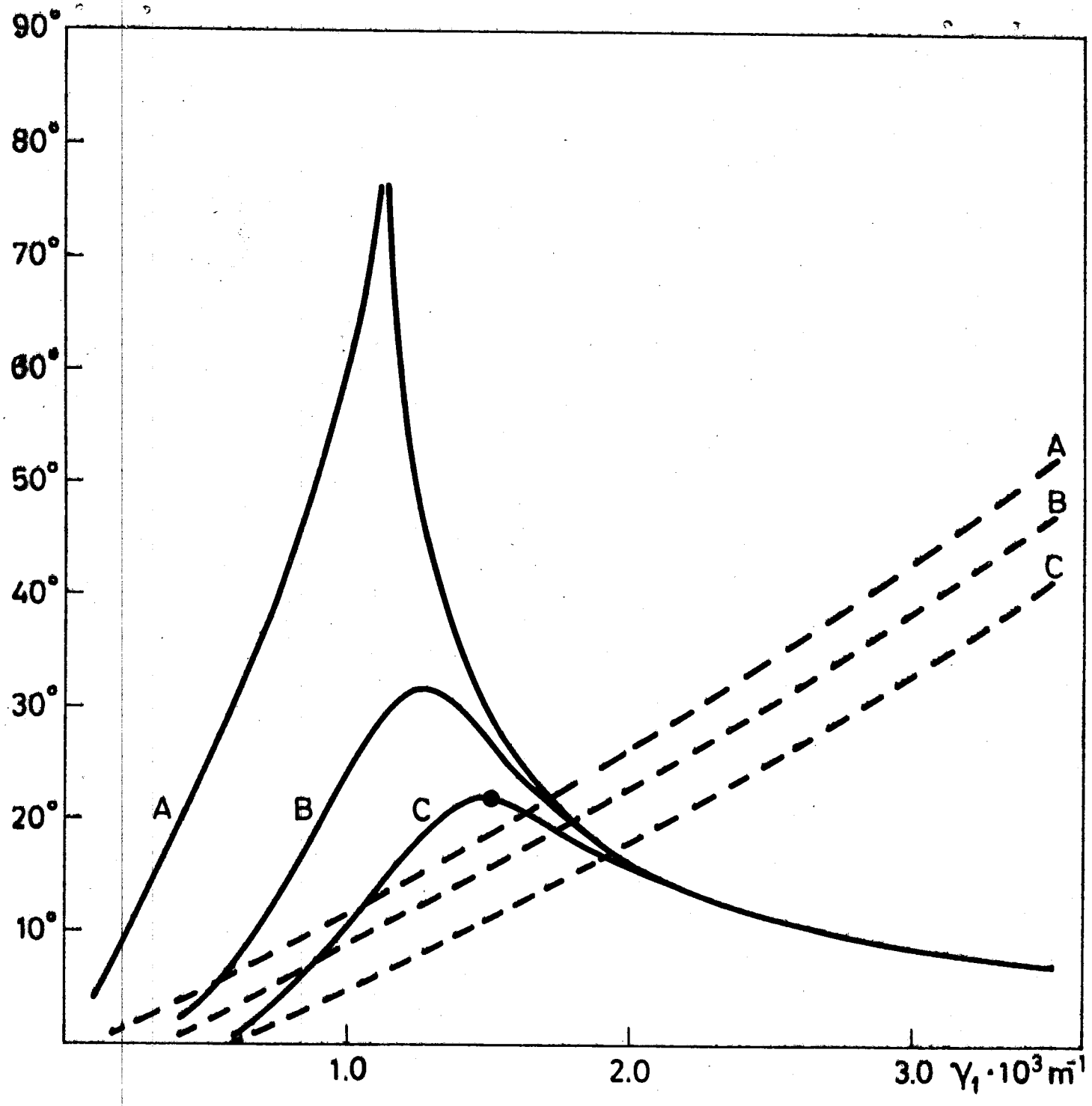

Fig. 4b

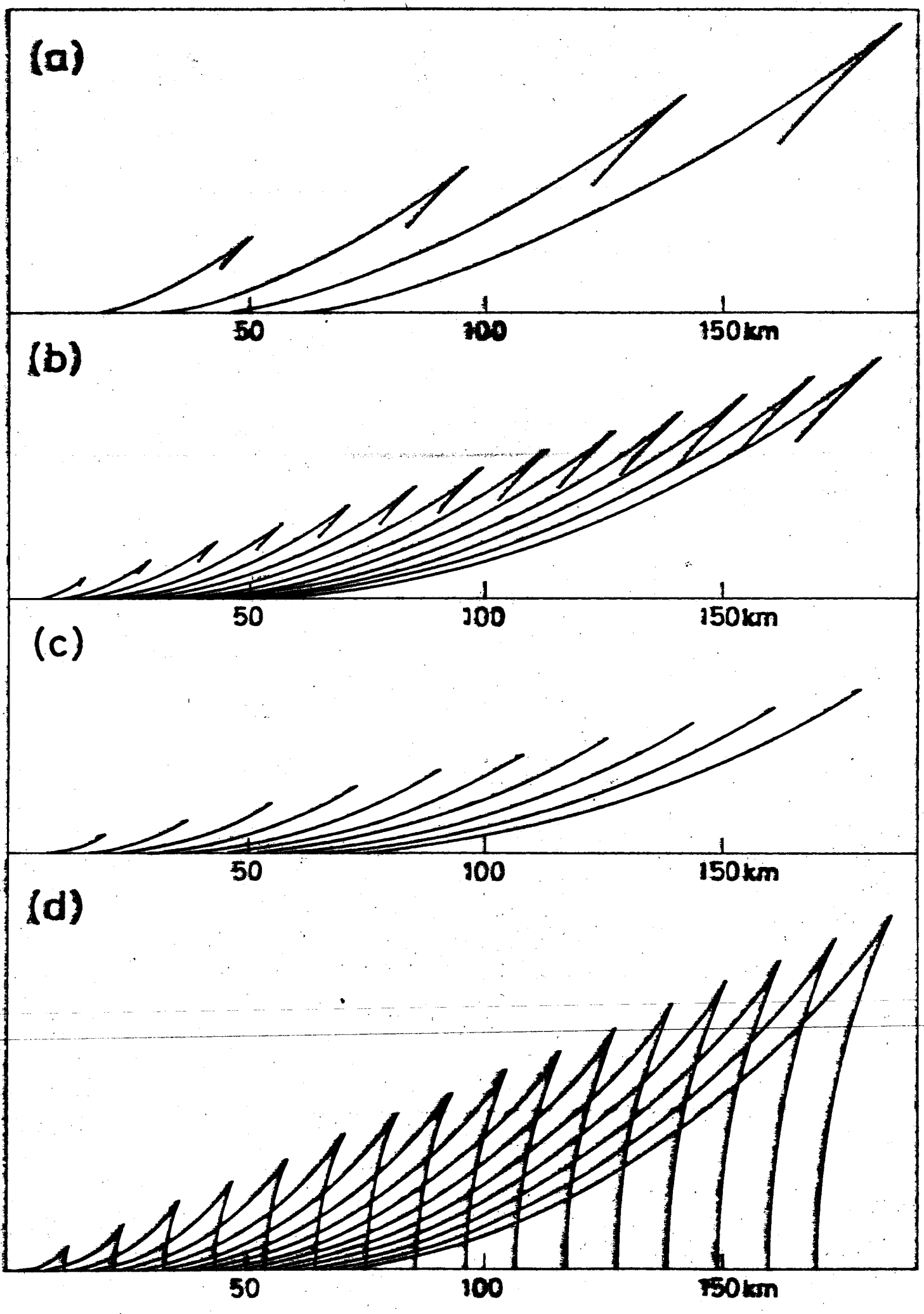

Fig. 5